JAERI-M
91-036

INITIAL EXPERIMENT OF FOCUSING WIGGLER OF MM WAVE FREE ELECTRON LASER ON LAX-I

March 1991

Keishi SAKAMOTO, Sunao MAEBARA, Akihiko WATANABE
Yasuaki KISHIMOTO, Hisako ODA*, Sunao KAWASAKI**
Takashi NAGASHIMA, Hikosuke MAEDA and Makoto SHIHO

日本原子力研究所
Japan Atomic Energy Research Institute

JAERI-Mレポートは，日本原子力研究所が不定期に公刊している研究報告書です。
入手の問合わせは，日本原子力研究所技術情報部情報資料課（〒319-11茨城県那珂郡東海村）あて，お申しこしください。なお，このほかに財団法人原子力弘済会資料センター（〒319-11 茨城県那珂郡東海村日本原子力研究所内）で複写による実費頒布をおこなっております。

JAERI-M reports are issued irregularly.
Inquiries about availability of the reports should be addressed to Information Division, Department of Technical Information, Japan Atomic Energy Research Institute, Tokai-mura, Naka-gun, Ibaraki-ken 319-11, Japan.

編集兼発行　日本原子力研究所
印　　刷　㈱原子力資料サービス

JAERI-M 91-036

Initial Experiment of Focusing Wiggler of MM Wave Free Electron Laser on LAX-1

Keishi SAKAMOTO, Sunao MAEBARA, Akihiko WATANABE
Yasuaki KISHIMOTO, Hisako ODA*, Sunao KAWASAKI**
Takashi NAGASHIMA, Hikosuke MAEDA and Makoto SHIHO

Department of Thermonuclear Fusion Research
Naka Fusion Research Establishment
Japan Atomic Energy Research Institute
Naka-machi, Naka-gun, Ibaraki-ken

(Received February 5, 1991)

Initial results of Free Electron Laser (FEL) Experiment in the mm wave region are presented.

The experiment is carried out using a induction linac system (LAX-1: Large current Accelerator Experiment) of E_b = 1 MeV, Ib = 1 ∿3 kA. The wiggler of FEL is composed of the curved surface magnets arrays (focusing wiggler), which is found to be effective for a transport of low energy and high current beam through the wiggler. The superradiance of the mm wave region (30 GHz ∿ 40 GHz) is observed. The growth rate of this radiation is 0.42 dB/cm.

Keywords: Free Electron Laser, Induction Linac, MM Wave Region, LAX-1, Focusing Wiggler, Superradiance (30 GHz ∿ 40 GHz), Growth Rate (0.42 dB/cm)

---

* Kanazawa Computer Service Corp.
** Saitama University

JAERI－M 91－036

LAX－1における収束型ウィグラーを用いたミリ波帯自由電子レーザー発振初期条件

日本原子力研究所那珂研究所核融合研究部
坂本　慶司・前原　　直・渡辺　聡彦
岸本　泰明・小田　久子*・川崎　　温**
永島　　孝・前田　彦佑・志甫　　諒

（ 1991 年 2 月 5 日受理 ）

ミリ波領域における自由電子レーザー（FEL）実験が，ビームエネルギー 1 MeV，ビーム電流 1～3 kA のインダクションライナック（LAX－1）を用いて行われた。

FELのウイグラーとしてハイパブリックサイン関数型の表面形状を持つビーム収束型永久磁石列が用いられ，これはウィグラー中の低エネルギー，大電流ビーム伝送に特に有効であることが示された。

また，これを用いたミリ波発振実験において，30GHz～40GHz帯ミリ波の発振が観測され，その成長率は 0.42 dB／cmであった。

那珂研究所：〒311－01 茨城県那珂郡那珂町大字向山 801－1
＊　カナザワコンピュータサービス ㈱
＊＊ 埼玉大学

Contents

目　　次

1. Introduction

JAERI started high power millimeter wave free electron laser project in 1988 for a plasma heating (ECRH) of JFT-2M tokamak using an induction linac accerelator. Construction of 5 MeV induction linac is planned in 1994, as the first step of the project, a prototype of the linac (LAX-1: Large Current Accerelator Experiment) was constructed, of which the beam energy is 1 MeV, diode current is 3 kA, and the pulse duration is 100 ns. And the initial experiment of FEL started in May of 1990 on LAX-1.

The main objective of the initial experiment is to study the beam transport in a low energy, high current region and to obtain data of superradiance for amplifier experiment of next stage.

When the wiggler is composed by the planar magnet array, the magnet with flat surface (or flat pole piece) has beed used. However, it was found with the simulation using a 3D code [brief discription is given in ref. 1] that the electron beam diverge drastically especially when an axial guide magnetic field is applied[2]. To suppress the beam divergence a focusing wiggler proposed by E. Sharleman[3], i.e., each permanent magnet has a surface of hyperbolic sinusoidal shape and form a magnetic field which work both for the wiggler and beam focusing, was constructed and tested.

In sec.II, a brief description on the beam dynamics in the wiggler is described; in sec.III, experimental apparatus is described; in sec.IV experimental results are presented. Some concluding remarks are summarized in sec.V.

2. Beam dynamics in the focusing wiggler

In the high current Raman regime FEL, a guiding field ($B_0\hat{e}_z$) is usually necessary to guide the electron beam. In this case, the horizontal divergence (x-direction) takes place for an off-axis particle when a beam is propagated through a planar wiggler and no equilibrium solution is found[4]. The beam divergence is due to $B_0\hat{e}_z\times(\partial|B_w(y)|/\partial y)\hat{e}_y$ drift motion in a transverse x-direction. To suppress the beam divergence, we employed a focusing wiggler. Figure 1 illustrates the focusing wiggler and the coordinate system. According

1. Introduction

JAERI started high power millimeter wave free electron laser project in 1988 for a plasma heating (ECRH) of JFT-2M tokamak using an induction linac accerelator. Construction of 5 MeV induction linac is planned in 1994, as the first step of the project, a prototype of the linac (LAX-1: Large Current Accerelator Experiment) was constructed, of which the beam energy is 1 MeV, diode current is 3 kA, and the pulse duration is 100 ns. And the initial experiment of FEL started in May of 1990 on LAX-1.

The main objective of the initial experiment is to study the beam transport in a low energy, high current region and to obtain data of superradiance for amplifier experiment of next stage.

When the wiggler is composed by the planar magnet array, the magnet with flat surface (or flat pole piece) has beed used. However, it was found with the simulation using a 3D code [brief discription is given in ref. 1] that the electron beam diverge drastically especially when an axial guide magnetic field is applied[2]. To suppress the beam divergence a focusing wiggler proposed by E. Sharleman[3], i.e., each permanent magnet has a surface of hyperbolic sinusoidal shape and form a magnetic field which work both for the wiggler and beam focusing, was constructed and tested.

In sec.II, a brief description on the beam dynamics in the wiggler is described; in sec.III, experimental apparatus is described; in sec.IV experimental results are presented. Some concluding remarks are summarized in sec.V.

2. Beam dynamics in the focusing wiggler

In the high current Raman regime FEL, a guiding field ($B_0\hat{e}_z$) is usually necessary to guide the electron beam. In this case, the horizontal divergence (x-direction) takes place for an off-axis particle when a beam is propagated through a planar wiggler and no equilibrium solution is found[4]. The beam divergence is due to $B_0\hat{e}_z\times(\partial|B_w(y)|/\partial y)\hat{e}_y$ drift motion in a transverse x-direction. To suppress the beam divergence, we employed a focusing wiggler. Figure 1 illustrates the focusing wiggler and the coordinate system. According

to E.T.Scharleman[3], the pole face is described by $y(x) = (1/k_y)\sinh^{-1}(c_0/\cosh k_x)$ where k_x and k_y satisfy the relation $k_x^2+k_y^2 = k_w^2$. The fieled strength produced by the focusing wiggler is given by $|\vec{B_w}| \sim B_w(1+r^2/2)$ near the axis for the equal focusing case, i.e. $k_x = k_y = k_w/\sqrt{2}$. Therefore, when the axial field $B_z\hat{e}_z$ is applied, a force $B_0\hat{e}_z\times\nabla(B_w) = B_0B_wr\hat{e}_\theta$ induces the beam rotation and the stable equilibrium solution of the electron beam is expected.

Beam trajectories in the wave guide (1.5×1.5 cm^2) are calculated with a 3D code and shown in Fig. 2 in the presence of the B_0 = 1.5 kG guiding field both for the planer wiggler and the focusing wiggler cases. The beam energy E_b = 1 MeV and the wiggler field B_w = 1.5 kG are chosen. At z = 0, we assume the circular beam cross section (r_b = 0.7 cm) with zero emittance. It is found that the elliptical cross section is roughly maintained for the focusing wiggler case, but the quick beam divergence is observed in the horizontal x-direction for the planer wiggler case.

3. Experimental Apparatus

Figure 3 shows the schematic figure of the experimental apparatus; induction linac, wiggler, and diagnostics.

Induction linac consists of four induction units, and each induction unit generates 250 kV pulse at the acceleration gap. Four stage units generate 1 MeV voltage at the diode. An electron beam is generated at the diode, which is field emission type, and the cathode material is velvet. Cathode diameter is 15 mm and the anode (tungsten mesh) diameter is 40 mm. Inside of each induction unit, guiding magnetic coil is equipped (inner coil). Maximum magnetic field strength is 3 kG and field ripple of the magnetic field is less than 5%. Outside of the induction linac, guiding magnetic coils are also equipped (outer coil) with the same maximum strength and ripple. The wiggler is installed inside of the outer coil.

The wiggler magnets are made of Nd-Fe-B permanent magnet. The surface shape is directly cut hyperbolic sinusoidal as illustrated in Fig. 1. The wiggler pitch is 5 cm and total pitch number is 30. The strength of the center wiggler field is 1∿2.5 kG, and it is changed by changing the gap distance. In the wiggler, the center field strength of the first 5

to E.T.Scharleman[3], the pole face is described by $y(x) = (1/k_y)\sinh^{-1}(c_0/\cosh k_x)$ where k_x and k_y satisfy the relation $k_x^2+k_y^2 = k_w^2$. The fieled strength produced by the focusing wiggler is given by $|\vec{B_w}| \sim B_w(1+r^2/2)$ near the axis for the equal focusing case, i.e. $k_x = k_y = k_w/\sqrt{2}$. Therefore, when the axial field $B_z\hat{e}_z$ is applied, a force $B_0\hat{e}_z\times\nabla(B_w) = B_0B_wr\hat{e}_\theta$ induces the beam rotation and the stable equilibrium solution of the electron beam is expected.

Beam trajectories in the wave guide (1.5×1.5 cm^2) are calculated with a 3D code and shown in Fig. 2 in the presence of the B_0 = 1.5 kG guiding field both for the planer wiggler and the focusing wiggler cases. The beam energy E_b = 1 MeV and the wiggler field B_w = 1.5 kG are chosen. At z = 0, we assume the circular beam cross section (r_b = 0.7 cm) with zero emittance. It is found that the elliptical cross section is roughly maintained for the focusing wiggler case, but the quick beam divergence is observed in the horizontal x-direction for the planer wiggler case.

3. Experimental Apparatus

Figure 3 shows the schematic figure of the experimental apparatus; induction linac, wiggler, and diagnostics.

Induction linac consists of four induction units, and each induction unit generates 250 kV pulse at the acceleration gap. Four stage units generate 1 MeV voltage at the diode. An electron beam is generated at the diode, which is field emission type, and the cathode material is velvet. Cathode diameter is 15 mm and the anode (tungsten mesh) diameter is 40 mm. Inside of each induction unit, guiding magnetic coil is equipped (inner coil). Maximum magnetic field strength is 3 kG and field ripple of the magnetic field is less than 5%. Outside of the induction linac, guiding magnetic coils are also equipped (outer coil) with the same maximum strength and ripple. The wiggler is installed inside of the outer coil.

The wiggler magnets are made of Nd-Fe-B permanent magnet. The surface shape is directly cut hyperbolic sinusoidal as illustrated in Fig. 1. The wiggler pitch is 5 cm and total pitch number is 30. The strength of the center wiggler field is 1~2.5 kG, and it is changed by changing the gap distance. In the wiggler, the center field strength of the first 5

pitches is adiabatically raised and the field strength of the rest of 25 pitches is kept constant as shown in Fig. 4.

Cylindrical wave guide of 28 mm diameter is used for the beam transimission through the wiggler. At the end of the wave guide, RF emission is observed, and Faraday cup was inserted to measure the transported current.

4. Experimental results and Discussions

4.1 Beam Transport

We first investigate the beam transport in the absence of the wiggler by changing the guiding field. Almost 80% of the current at the entrance aperture was found to be transported to the end of the wave guide when the field strength is changed between B_0 = 1.5∿3.0 kG in each of inner and outer coil. The beam diameter was kept almost constant in the series of experiments (15-20 mm).

When the wiggler was attached, we found the degradation of the beam current down to 200 A at the entrance aperture. The degradation may result from the fringe field of B_y component due to the magnetization of the yoke. About δB_y = 1.0 kG fringe field was observed at the wiggler entrance. When the fringe field was reduced by changing the shape of the yoke, we observed an increment of the entrance current up to 300 A.

Typical example of the beam transport profile measured by a Farady-cup is shown by open circle in Fig. 5 for the guiding field of 2.9 kG in wiggler section. About 30-50% of the current was found to be transported to the end of wiggler. It was also found the accessible window for the guiding field which permits the beam transport is narrower than the case of no wiggler.

The closed circle in Fig. 5 shows the beam current when the adiabatic taper is absent. The adiabatic taper region is essential for the beam injection into the wiggler.

4.2 Superradiance

A superradiance of millimeter wave was observed. The output power was sampled by the horn antenna having an aperture of 37 mm × 47 mm located 25 cm apart from the wave guide and was measured

pitches is adiabatically raised and the field strength of the rest of 25 pitches is kept constant as shown in Fig. 4.

Cylindrical wave guide of 28 mm diameter is used for the beam transimission through the wiggler. At the end of the wave guide, RF emission is observed, and Faraday cup was inserted to measure the transported current.

4. Experimental results and Discussions

4.1 Beam Transport

We first investigate the beam transport in the absence of the wiggler by changing the guiding field. Almost 80% of the current at the entrance aperture was found to be transported to the end of the wave guide when the field strength is changed between B_0 = 1.5∿3.0 kG in each of inner and outer coil. The beam diameter was kept almost constant in the series of experiments (15-20 mm).

When the wiggler was attached, we found the degradation of the beam current down to 200 A at the entrance aperture. The degradation may result from the fringe field of B_y component due to the magnetization of the yoke. About δB_y = 1.0 kG fringe field was observed at the wiggler entrance. When the fringe field was reduced by changing the shape of the yoke, we observed an increment of the entrance current up to 300 A.

Typical example of the beam transport profile measured by a Farady-cup is shown by open circle in Fig. 5 for the guiding field of 2.9 kG in wiggler section. About 30-50% of the current was found to be transported to the end of wiggler. It was also found the accessible window for the guiding field which permits the beam transport is narrower than the case of no wiggler.

The closed circle in Fig. 5 shows the beam current when the adiabatic taper is absent. The adiabatic taper region is essential for the beam injection into the wiggler.

4.2 Superradiance

A superradiance of millimeter wave was observed. The output power was sampled by the horn antenna having an aperture of 37 mm × 47 mm located 25 cm apart from the wave guide and was measured

by the crystal detectors. The frequency was analyzed by the band pass filters and the cut-off wave guides. The typical time sequence of the beam current and the output power are shown in Fig. 6. These data were obtained at the condition of $E_b \lesssim 1$ MeV, the wiggler field B_w = 1.25 kG, and the guiding field of B_0 = 2.9 kG. The obtained RF power in the figure includes the frequency all above 32 GHz. The power is about 5 W. The polarization of the radiation was measured by rotating the horn antenna, and the ratio of $(E_y/E_x)^2$ was among 0∿0.16 in the series of the experiments. Here, E_x is electric field of parallel direction to the wiggler field and E_y is that of perpendicular direction both to the E_x and the axis of the drift tube.

In order to obtain the frequency spectrum, we measured the integrated power by changing the cut-off frequency of the detection wave guide. Figure 7 shows the integrated power spectrum If (solid line), and the power spectrum P(f) (dashed line). In this figure, deduced spectrum peak locates around 40 GHz which agrees with the value by the 3D simulation.

To estimate the growth rate of the radiation, the output power was measured as a function of the interaction length. Here, the electron beam was terminated by placing the additional magnet near the wave guide. By changing the position of the magnet, the interaction length can be changed. As the result, the growth rate of the radiation of 0.42 dB/cm was obtained as shown in Fig. 8, which coincides with the simulated value of the 3D code.

5. Concluding Remarks

The experimental results with the focusing wiggler are summarized as;

1) About 100 A current is transported in the focusing wiggler, with the transportation efficiency of about 30-50%.
2) Adiabatic taper region is essential for the beam transportation.
3) Super radiant emission spectrum is observed with the spectral peak at about 40 GHz.
4) Integrated radiation power between 30 GHz and 55 GHz was about 5 W and the observed growth rate was 0.42 dB/cm.
5) In the series of experiments, the ratio of $(E_y/E_x)^2$ is almost

by the crystal detectors. The frequency was analyzed by the band pass filters and the cut-off wave guides. The typical time sequence of the beam current and the output power are shown in Fig. 6. These data were obtained at the condition of $E_b \lesssim 1$ MeV, the wiggler field B_w = 1.25 kG, and the guiding field of B_0 = 2.9 kG. The obtained RF power in the figure includes the frequency all above 32 GHz. The power is about 5 W. The polarization of the radiation was measured by rotating the horn antenna, and the ratio of $(E_y/E_x)^2$ was among 0∿0.16 in the series of the experiments. Here, E_x is electric field of parallel direction to the wiggler field and E_y is that of perpendicular direction both to the E_x and the axis of the drift tube.

In order to obtain the frequency spectrum, we measured the integrated power by changing the cut-off frequency of the detection wave guide. Figure 7 shows the integrated power spectrum If (solid line), and the power spectrum P(f) (dashed line). In this figure, deduced spectrum peak locates around 40 GHz which agrees with the value by the 3D simulation.

To estimate the growth rate of the radiation, the output power was measured as a function of the interaction length. Here, the electron beam was terminated by placing the additional magnet near the wave guide. By changing the position of the magnet, the interaction length can be changed. As the result, the growth rate of the radiation of 0.42 dB/cm was obtained as shown in Fig. 8, which coincides with the simulated value of the 3D code.

5. Concluding Remarks

The experimental results with the focusing wiggler are summarized as;

1) About 100 A current is transported in the focusing wiggler, with the transportation efficiency of about 30-50%.
2) Adiabatic taper region is essential for the beam transportation.
3) Super radiant emission spectrum is observed with the spectral peak at about 40 GHz.
4) Integrated radiation power between 30 GHz and 55 GHz was about 5 W and the observed growth rate was 0.42 dB/cm.
5) In the series of experiments, the ratio of $(E_y/E_x)^2$ is almost

among 0 ∿ 0.16, which shows the almost linearly polarized field. The finite E_y component is considered to be caused by the wiggler motion in a y-direction induced by the presence of the guiding field.

guiding field may be also the possible candidate.

Although the focusing wiggler concept was firstly proposed for the high energy electron beam such as $\gamma \cong 100$ and no guiding field case, we verify that the focusing wiggler becomes indispensable for the beam transport when beam energy is low ($\gamma \cong 3$) and the guiding field is not zero. The simulation result shows that the the beam rotation induced by the focusing and guiding fields dose not lead to the electron phase mismatch with the radiation field. This is verified experimentally that the observed growth rate 0.42 dB/cm is coincides with the simulation value. These points are considered to be important when we work in the case with high current beam and with low beam energy $1 \leq E_b \leq 5$ MeV, where we sometimes use the guiding magnetic field.

References

(1) T.J. Orzechowski, B.R. Anderson, J.C. Clark, W.M. Fawley, A.C. Prosniz, E.T. Sharlemann, S.M. Yarema, D.B. Hopkins, A. Sessler, J.S. Wurtele; Phys. Rev. Lett. 57(1986)892.

(2) Y. Kisimoto, H. Oda, and M. Shiho; Phys. Rev. Lett. 65(1990)851.

(3) M. Shiho, Y. Kishimoto, K. Sakamoto, S. Maebara, K. Odajima, H. Maeda, T. Nagashima, N. Kobayashi, A. Watanabe, and S. Kawasaki; The 2nd. Int. Symp. on Advanced Nucl. Ener. Res., Jan. 24-26, 1990 p476-p481, Organzed by JAERI, Atom. Ene. Soc, and of Japan, The Phy. Soc of Japan.

(4) E.T. Scharleman, J. Appl. Phys. 58(1985)2154.

(5) J.A. Pasour, F. Maka, and C.W. Roberson; J. Appl. Phys. 53(1982) 717.

among 0 ∿ 0.16, which shows the almost linearly polarized field. The finite E_y component is considered to be caused by the wiggler motion in a y-direction induced by the presence of the guiding field.

guiding field may be also the possible candidate.

Although the focusing wiggler concept was firstly proposed for the high energy electron beam such as $\gamma \cong 100$ and no guiding field case, we verify that the focusing wiggler becomes indispensable for the beam transport when beam energy is low ($\gamma \cong 3$) and the guiding field is not zero. The simulation result shows that the the beam rotation induced by the focusing and guiding fields dose not lead to the electron phase mismatch with the radiation field. This is verified experimentally that the observed growth rate 0.42 dB/cm is coincides with the simulation value. These points are considered to be important when we work in the case with high current beam and with low beam energy $1 \leq E_b \leq 5$ MeV, where we sometimes use the guiding magnetic field.

References

(1) T.J. Orzechowski, B.R. Anderson, J.C. Clark, W.M. Fawley, A.C. Prosniz, E.T. Sharlemann, S.M. Yarema, D.B. Hopkins, A. Sessler, J.S. Wurtele; Phys. Rev. Lett. 57(1986)892.

(2) Y. Kisimoto, H. Oda, and M. Shiho; Phys. Rev. Lett. 65(1990)851.

(3) M. Shiho, Y. Kishimoto, K. Sakamoto, S. Maebara, K. Odajima, H. Maeda, T. Nagashima, N. Kobayashi, A. Watanabe, and S. Kawasaki; The 2nd. Int. Symp. on Advanced Nucl. Ener. Res., Jan. 24-26, 1990 p476-p481, Organzed by JAERI, Atom. Ene. Soc, and of Japan, The Phy. Soc of Japan.

(4) E.T. Scharleman, J. Appl. Phys. 58(1985)2154.

(5) J.A. Pasour, F. Maka, and C.W. Roberson; J. Appl. Phys. 53(1982) 717.

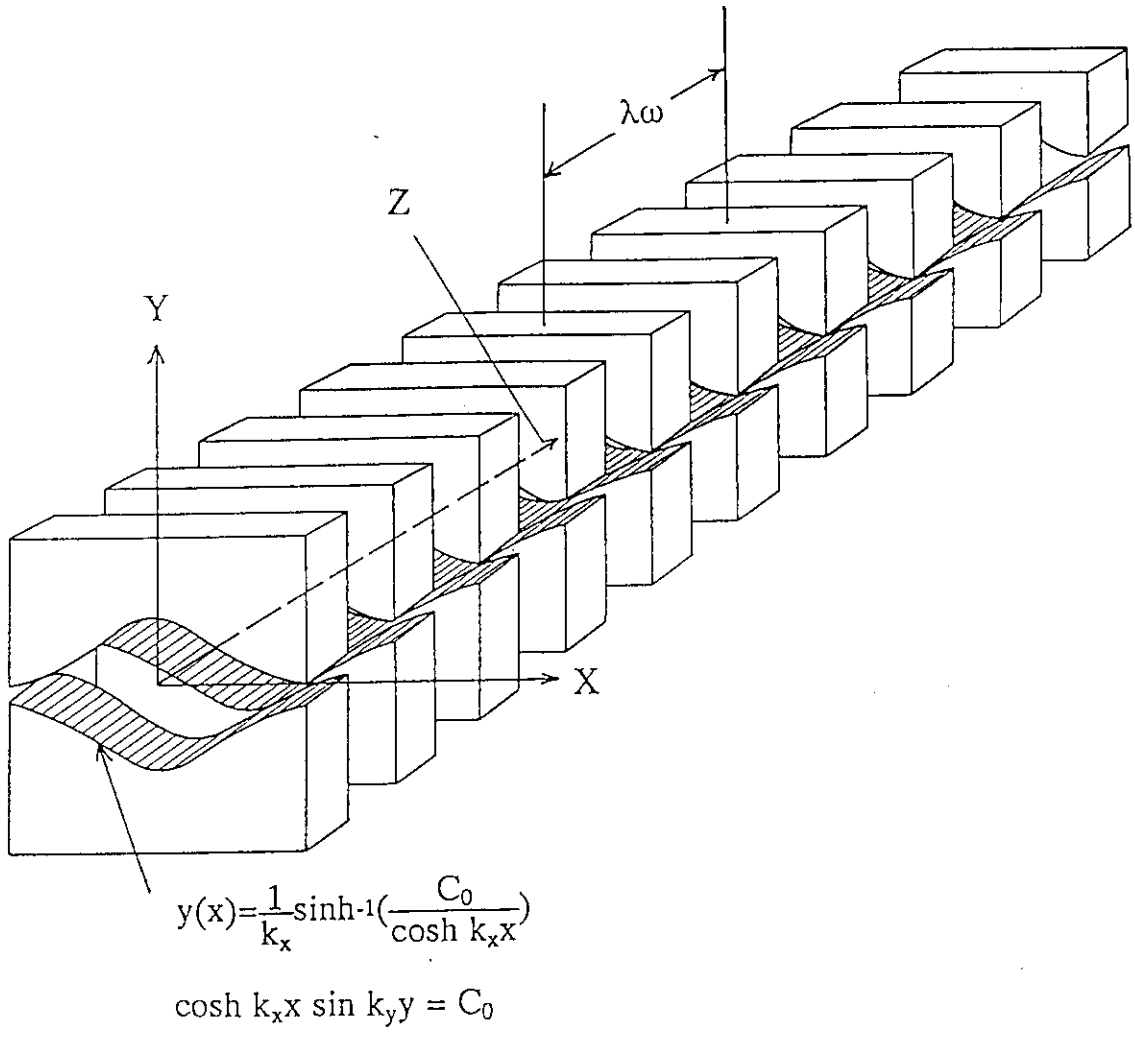

Fig.1 Focusing Wiggler and coordinate system.

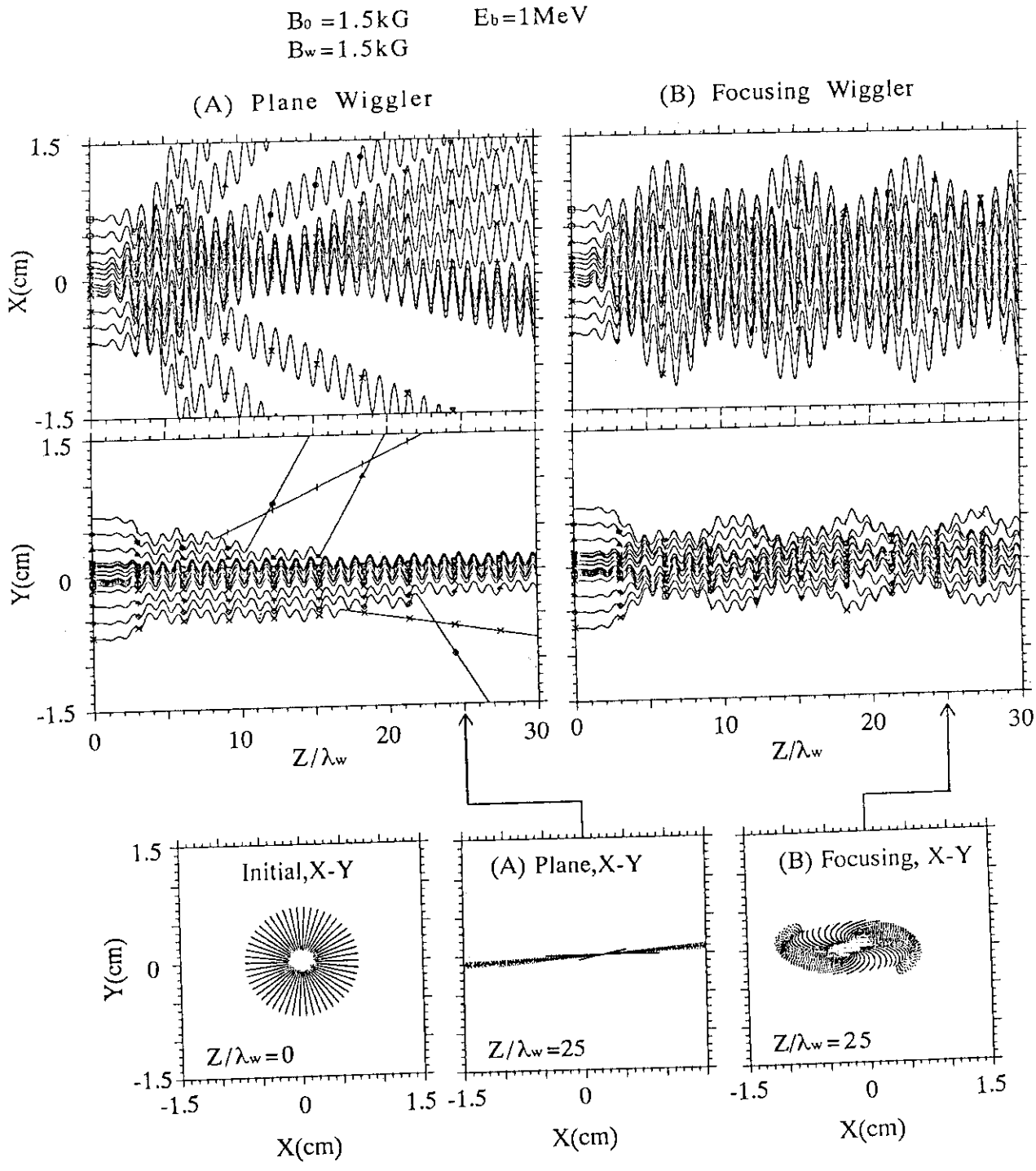

Fig.2 Beam trajectories in the case of both planes and focusing wiggler.
Upper: Two figures show X-Z projection for each case.
Middle: Two figure show Y-Z projection.
Lower: Three figure show X-Y projection at the initial(left) and middle point Z/λ_w=25 alonthe Z axis.
Simulation was performed until Z/λ_w reaches 50.

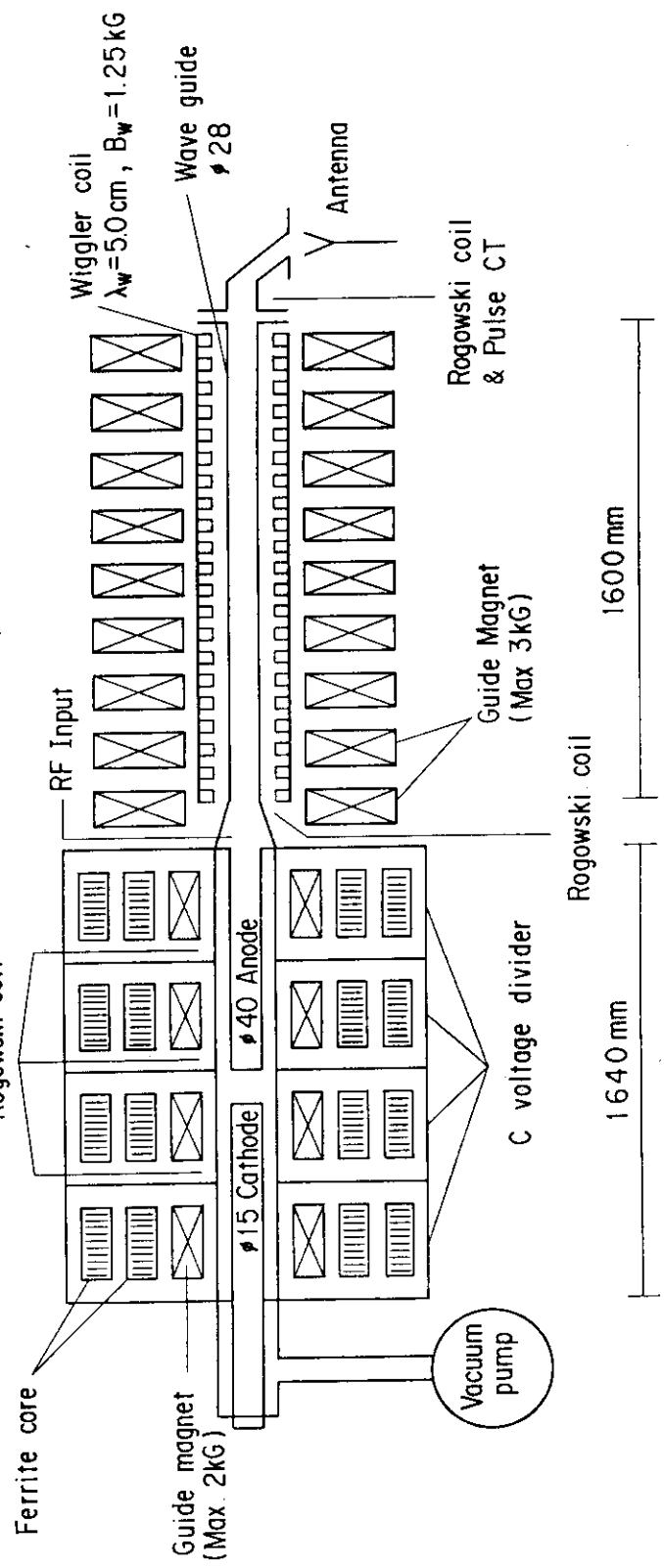

Fig.3 Schematics of the experimental apparatus.

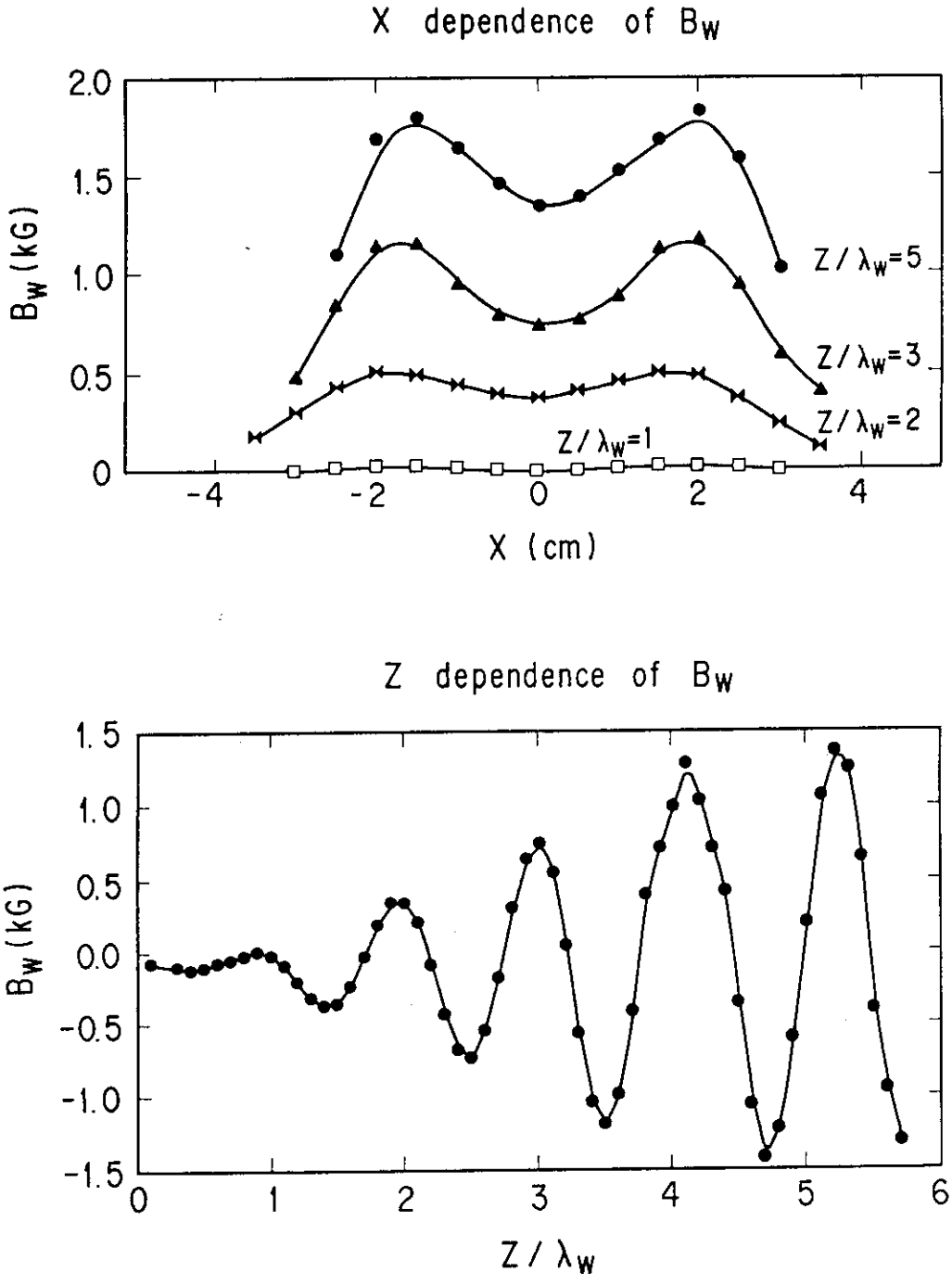

Fig.4 Shape of magnetic field strength of Bw in the adiabatic taper region.

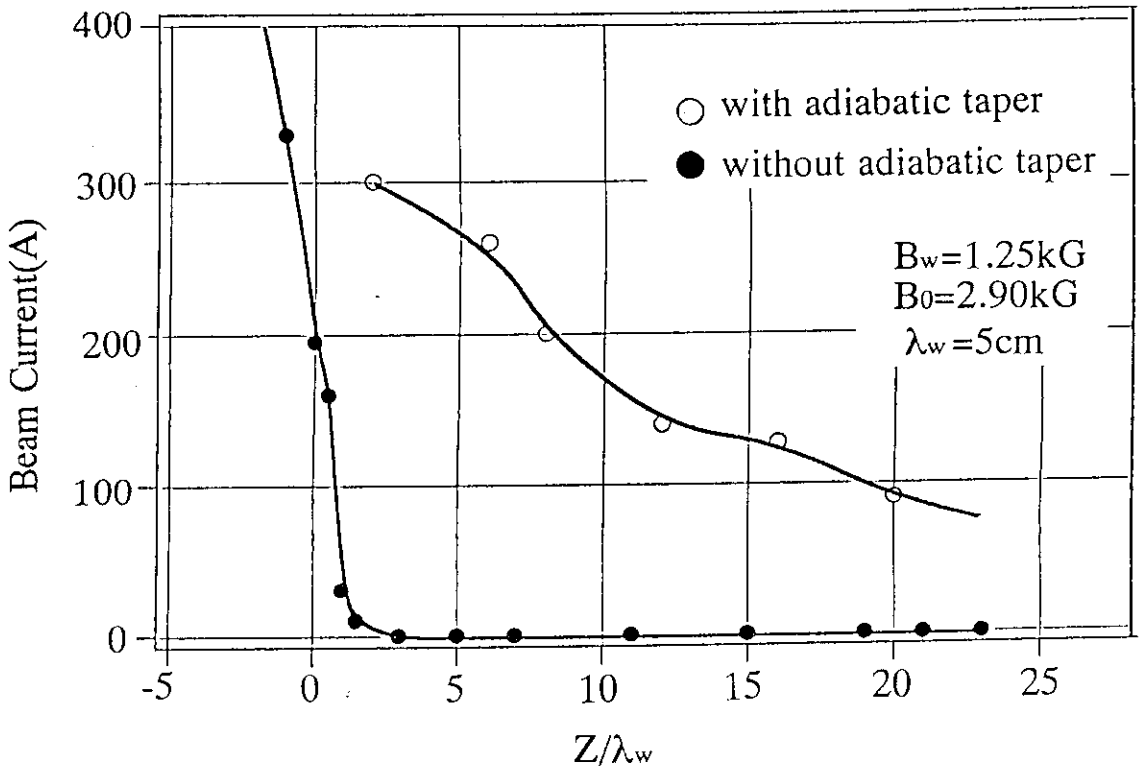

Fig.5 Typical example of current transport profile along Z axis of the wiggler.

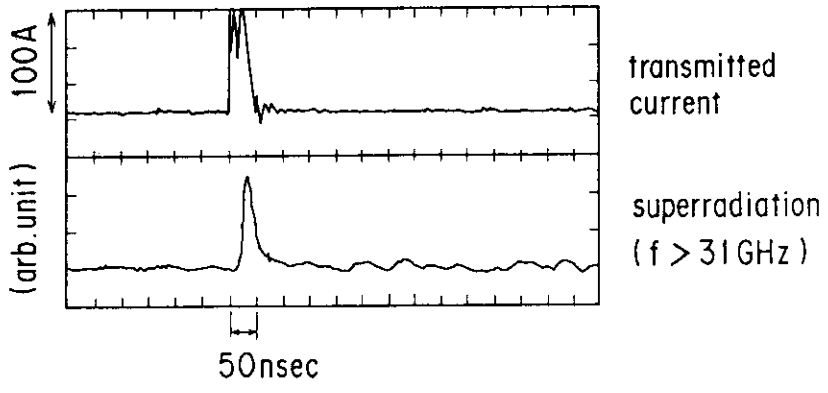

Fig.6 Wave form of the super radiation.

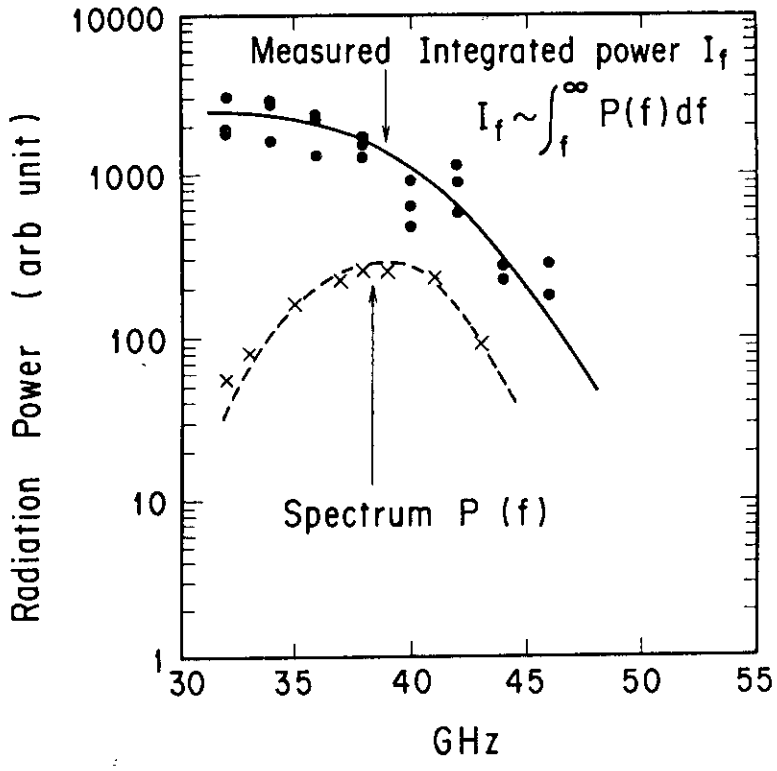

Fig.7 Spectrum of super radiation.

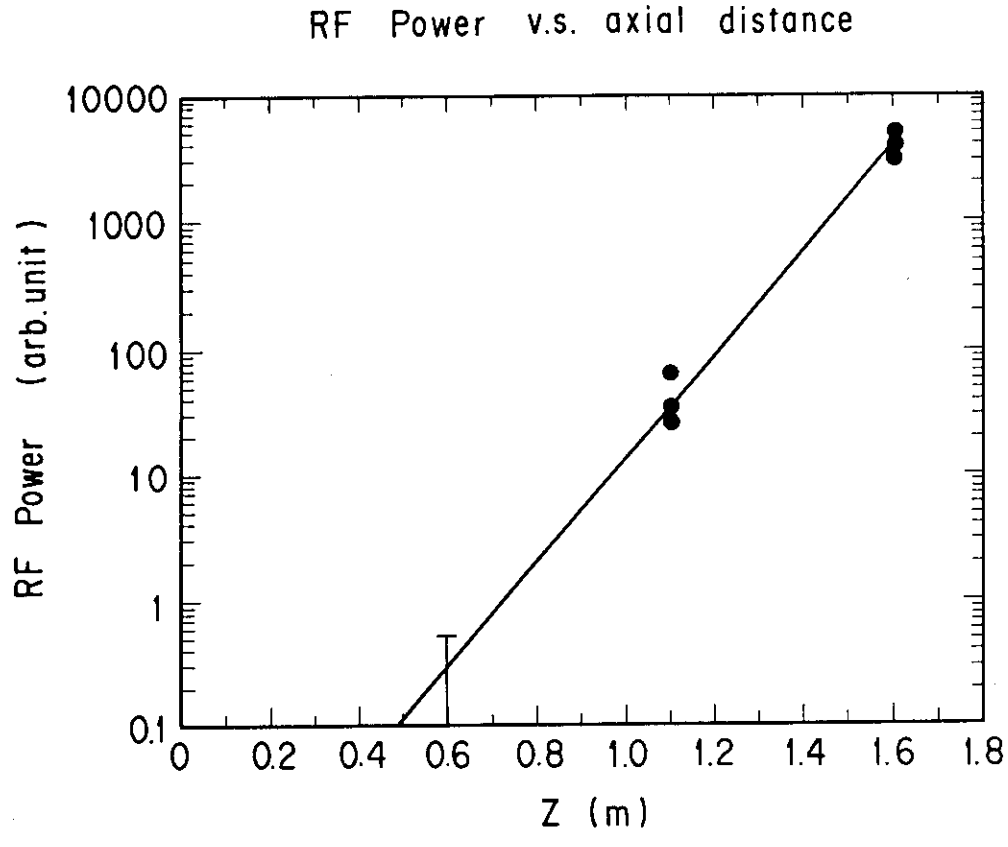

Fig.8 Relation between radiation power and integration length.